Li et al. BMC Medical Imaging (2024) 24:288
https://doi.org/10.1186/s12880-024-01465-4

BMC Medical Imaging

RESEARCH

Open Access

CT coronary fractional flow reserve based on artificial intelligence using different software: a repeatability study

Jing Li[1†], Zhenxing Yang[1†], Zhenting Sun[1], Lei Zhao[1*], Aishi Liu[1*], Xing Wang[2], Qiyu Jin[3] and Guoyu Zhang[3]

Abstract

Objective This study aims to assess the consistency of various CT-FFR software, to determine the reliability of current CT-FFR software, and to measure relevant influence factors. The goal is to build a solid foundation of enhanced workflow and technical principles that will ultimately improve the accuracy of measurements of coronary blood flow reserve fractions. This improvement is critical for assessing the level of ischemia in patients with coronary heart disease.

Methods 103 participants were chosen for a prospective research using coronary computed tomography angiography (CCTA) assessment. Heart rate, heart rate variability, subjective picture quality, objective image quality, vascular shifting length, and other factors were assessed. CT-FFR software including K software and S software are used for CT-FFR calculations. The consistency of the two software is assessed using paired-sample t-tests and Bland-Altman plots. The error classification effect is used to construct the receiver operating characteristic curve.

Results The CT-FFR measurements differed significantly between the K and S software, with a statistical significance of $P < 0.05$. In the Bland-Altman plot, 6% of the points (14 out of 216) fell outside the 95% consistency level. Single-factor analysis revealed that heart rate variability, vascular dislocation offset distance, subjective image quality, and lumen diameter significantly influenced the discrepancies in CT-FFR measurements between two software programs ($P < 0.05$). The ROC curve shows the highest AUC for the vessel shifting length, with an optimal cut-off of 0.85 mm.

Conclusion CT-FFR measurements vary among software from different manufacturers, leading to potential misclassification of qualitative diagnostics. Vessel shifting length, subjective image quality score, HRv, and lumen diameter impacted the measurement stability of various software.

Keywords Coronary flow reserve fraction, Difference, Reliability, Influencing factors

[†]Jing Li and Zhenxing Yang contributed equally and are co-first authors.

*Correspondence:
Lei Zhao
281005117@qq.com
Aishi Liu
liuas2024@163.com
Full list of author information is available at the end of the article

Background

Coronary artery disease (CAD) is a well-documented risk factor for mortality and morbidity of cardiovascular diseases among adults [1]. Coronary heart disease requires a comprehensive evaluation of morphological and hemodynamic information of coronary arteries [2, 3]. Currently, invasive fractional flow reserve (iFFR) is a crucial clinical benchmark for assessing the function of coronary artery disease (CAD) [4]. CT fractional flow reserve (CT-FFR) is a valuable method that utilizes computational fluid dynamics (CFD) to identify and assess ischemic lesions resulting from coronary artery stenosis. It is also effective in reclassifying the severity of myocardial ischemia [5–7].

The use of a fluid mechanics model requires considerable computing resources for the simulation of what can often be large and complex systems [8–10]. Advances in technology have led to the implementation of artificial intelligence in CT-FFR. This involves extracting clinical data characteristics using machine learning or deep learning algorithms to achieve autonomous, rapid, and precise processing [11–13]. Different software vendors vary in technical areas such as architecture, artificial intelligence, algorithms, training, and other variables. The variations in these elements could indicate ambiguity in the results obtained [14, 15]. Hence, various software programs may result in varying identification of a certain ischemia injury.

We conducted a thorough literature review and did not find any studies comparing various CT-FFR software. Furthermore, the CT-FFR assessment can be influenced by pathophysiology, picture quality, scanning settings, and other factors. Therefore, there is an urgent need for a comprehensive and systematic study of the differences in the CT-FFR measurements and to identify the factors, so as to improve the reliability and accuracy of the CT-FFR and provide strong support for its accurate assessment of myocardial ischemic lesions. Hence, this study aims to evaluate the consistency between different CT-FFR measurement softwares and identify relevant influence factors.

Materials and methods

Study population

This retrospective investigation was approved by the institutional ethics committee, which provided a waiver of informed consent. 103 patients suspected of having coronary artery disease (CAD) were chosen in advance from our hospital between June 2020 and July 2021. The median age of the participants was 52 years, ranging from 22 to 82 years, with 61 males and 42 females.

Inclusion criteria: Patients with suspected coronary artery disease necessitating coronary computed tomography angiography (CCTA).

Exclusion criteria include data not meeting analysis requirements, poor breath holding, previous iodine allergy, renal insufficiency (serum creatinine $\geq$ 120 μmol/L), severe tachycardia or arrhythmia, suspected acute coronary syndrome, complex congenital heart disease, and cardiac device implantation.

CCTA data acquisition

Patient preparation

An 18-gauge catheter (BD Intima II 18G, BD, Jiangsu, China) was inserted into the elbow vein, and its functionality was confirmed by flushing 20 mL of physiological saline before injecting the contrast agent. Patients having a heart rate over 70 beats per minute were given Betaloc tablets from Yangzi Pharmaceutical in China at an oral dosage ranging from 25 to 75 mg, as shown in Fig. 1.

Scan protocol

The CCTA examinations were conducted using a 128-slice dual-source CT scanner (SOMATOM Definition Flash, Siemens Medical Solutions, Forchheim, Germany) with the patient lying down in a supine posture with their feet first. The bolus tracking technique is employed for automatic triggering. The monitoring point was located 1 cm below the tracheal carina. The area of interest (ROI) was delineated at the aortic root. The drawing range was located in the lower center of the aortic root, distant from the superior vena cava and pulmonary artery. The trigger level was established at 100 Hounsfield units (HU). Following the summit, there is a 5-second delay in the CCTA images. A prospective ECG acquisition sequence technique was used for CCTA to capture data during the 35 − 80% of the R-R interval.

Acquisition parameters: Tube voltage set at 70 kVp; tube current at 320 mAs per rotation using ATCM (CareDose 4D, Siemens Medical Solutions, Forchheim, Germany). The detector collimation measured $2 \times 64 \times 0.6$ mm and the gantry rotation time was 280 ms. The axial image reconstruction has a thickness of 0.75 mm and a reconstruction interval of 0.6 mm. Image reconstruction was performed using sinogram-affirmed iterative reconstruction (SAFIRE 3, Siemens Medical Solutions, Forchheim, Germany) and a medium smooth convolution kernel (I26f).

The experts recommended favoring the middle ventricular diastolic phase, which corresponds to the 60–80% phase of the R-R interval. Individuals with low to medium heart rates often choose a 70–80% phase

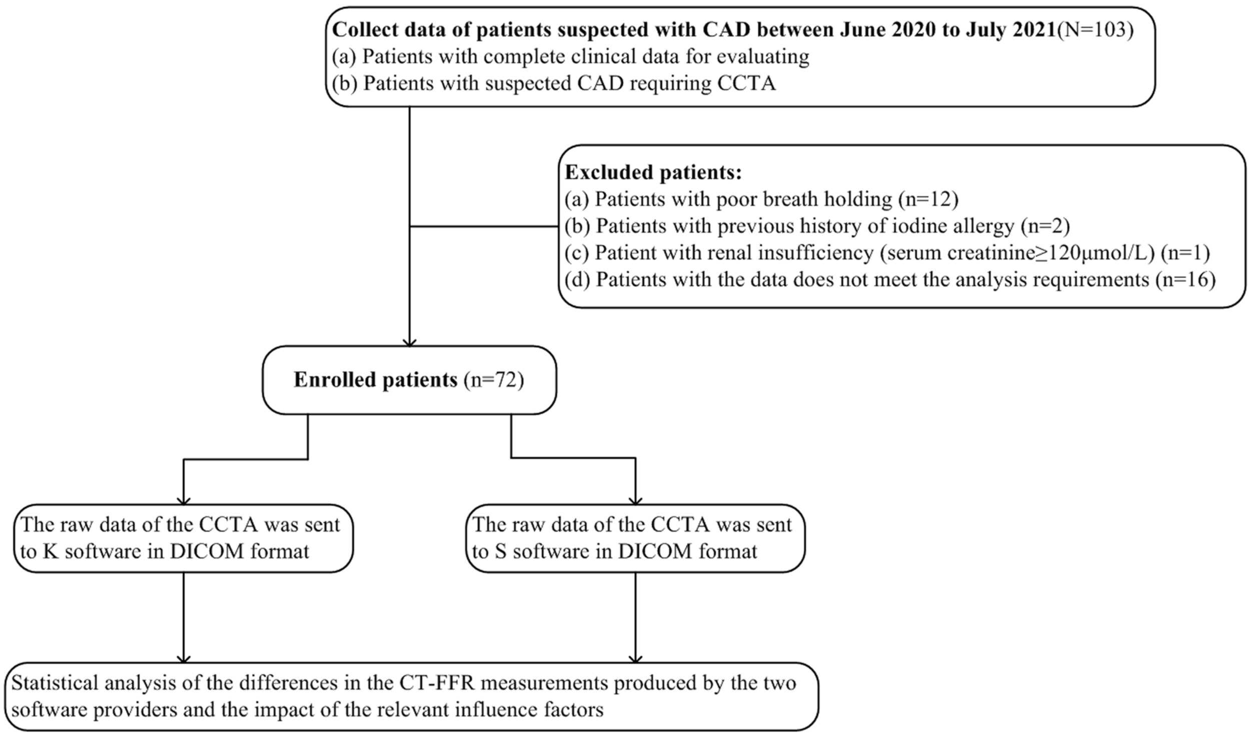

Fig. 1 Recruitment flowchart for including patients in the study and technology roadmap

reconstruction of the R-R interval [16]. We chose the optimal diastolic data that was automatically reconstructed by the CT equipment for analysis. The data was uploaded to an image post-processing workstation (ADW version 4.5, GE healthcare, Milwaukee, WI, USA) and the CT-FFR professional analysis platform.

Contrast injection

Iodixanol Injection 370 mgI/mL from Bayer Schering Pharma AG Guangzhou branch in Guangdong, China is used as the contrast agent for CCTA. The injection volume was adjusted to 50–70 mL at a rate of 4.0-5.5 mL/sec based on the individual's body weight. After administering the contrast injection, 40 mL of physiological saline was flushed.

Image post-processing

Post-processing of the image was conducted using a sophisticated workstation (ADW version 4.5, GE healthcare, Milwaukee, WI, USA). Curved planar reconstruction (CPR), maximum intensity projection (MIP), volumetric rendering technique (VRT), and multi-planar reformation (MPR) were used to assess the coronary arteries. Image quality, stenosis, and lumen diameter were assessed using multiplanar reformation (MPR) and axial views of each channel.

Image quality

Subjective evaluation

Based on the 'vessel' level, including left anterior descending (LAD), left circumflex (LCx) and right coronary artery (RCA), the image quality was assessed by two independent observers (with 8 and 10 years of cardiovascular diagnostic experience, respectively) blinded to each patient on the workstation independently. We use a scale with four levels. Image quality was rated as outstanding (scores 3 and 4) and inferior (scores 1 and 2). The two witnesses resolved their disagreement by consulting with each other to reach a consensus, as shown in Fig. 2.

Attenuation, noise, signal-to-noise ratio and contrast-to-noise ratio

The average and variability of the aortic root (AO), left coronary artery (LCA), and RCA were determined using areas of interest (ROIs). The standard deviation (SD) served as the noise. The mean attenuation was measured in the adipose tissue around the ascending aorta as the background signal. ROIs drew the largest area as much

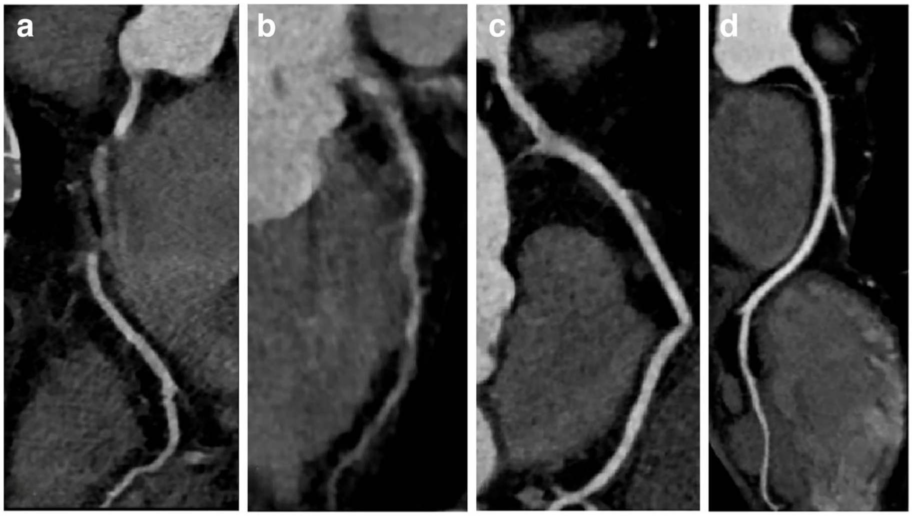

Fig. 2 Subjective assessment of the image quality score. Note: 1 = poor, unavailable; 2 = acceptable, moderate artifact, but images are available; 3 = good, slight artifact; and 4 = excellent, no visible artifact. Figure **a** ~ **d** showed the image quality scores of 1, 2, 3 and 4, respectively

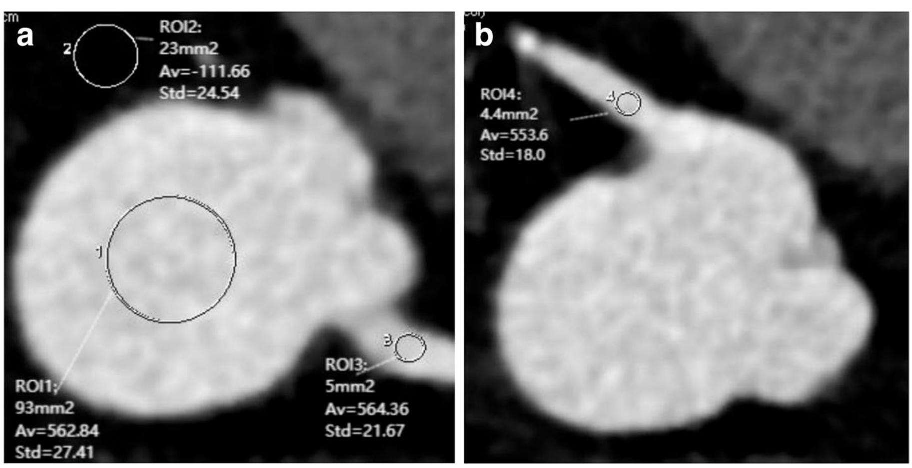

Fig. 3 Objective image quality measurement. Note: Figure **a** showed the mean values and standard deviation of the aortic root, left coronary artery and adipose tissue area around the aortic root as attenuation and noise, respectively; figure **b** showed the mean attenuation and noise of the right coronary artery

as possible. The signal-to-noise ratio (SNR) and contrast-to-noise ratio (CNR) were calculated by the formula, as shown in Fig. 3:

$$\mathrm{SNR} = \mathrm{Meanattenuation/Noise} \quad (1)$$

$$\mathrm{CNR} = (\text{Mean attenuation - Mean attenuation of adipose tissue around the AO})/\text{Noise}] \quad (2)$$

Vessel shifting length

The unregistered phenomena of vascular data included the vascular truncation, dislocation and stepped artifacts. This phenomenon mainly occurs during arrhythmia. In order to quantify the severity of the non-registration of different phases, we defined a new index, viz., vessel shifting length (VSL). The measurement rules of VSL are shown in Fig. 4.

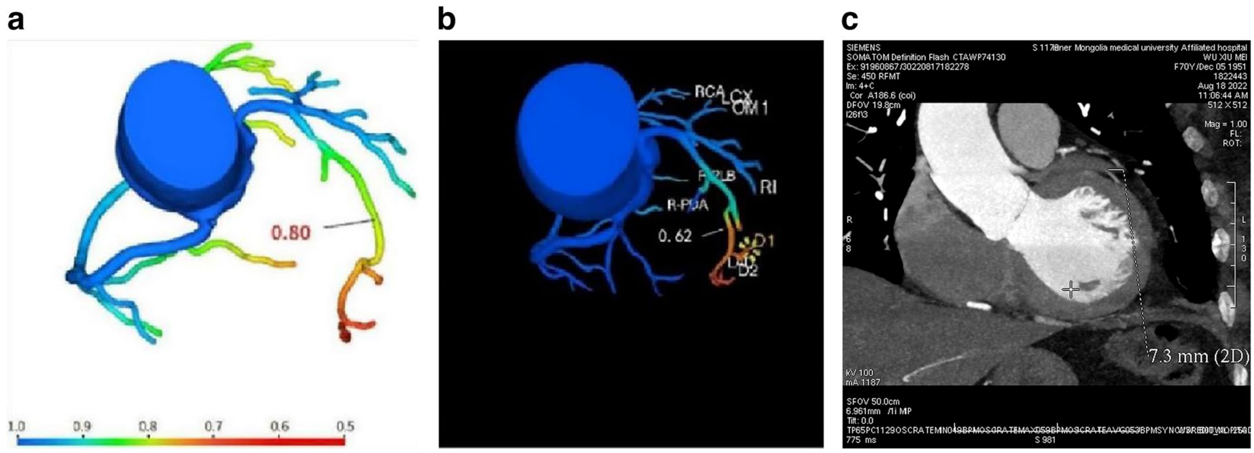

Fig. 4 Schematic representation of the CT-FFR measurement. Note: MPR for coronary artery data and a suitable oblique coronary position were determined to measure the maximum shifting length of vessels (Fig. 4c). The VSL of LAD was 7.3 mm, CT-FFR = 0.80 determined by K software (Fig. 4a), and CT-FFR = 0.62 determined by S software (Fig. 4b). The measurement results were qualitatively inconsistent with the diagnosis

Table 1 Coronary stenosis

CAD-RADS grading	Degree of stenosis
CAD-RADS 0	0% (No visible stenosis)
CAD-RADS 1	1–24% (Minimal stenosis)
CAD-RADS 2	25–49% (Mild stenosis)
CAD-RADS 3	50–69% (Moderate stenosis)
CAD-RADS 4	70–99% (Severe stenosis)
CAD-RADS 5	100% (Occluded)

Measurement of the lumen diameter
Following magnetic resonance imaging (MPR) of the coronary artery, the diameter of the proximal lumen of the primary coronary arteries (LAD, LCx, and RCA) was quantified as the lumen diameter (LD) [17].

Coronary stenosis
Coronary stenosis was assessed by two obstetricians with 8 and 10 years of experience in cardiovascular diagnostics. The evaluation method involves the diameter method, which is calculated as follows.

The formula to calculate the degree of vascular stenosis is: (D-d) / D × 100%, where d represents the average value of the normal lumen diameter at both ends of the stenosis, and D is the smallest lumen diameter at the stenosis. The severity of narrowing was assessed based on SCCT guidelines, as shown in Table 1 [16, 18].

CT-FFR
The CT-FFR calculation was performed using CT-FFR software, which included K software (deep vessel FFR, KEYA medical, Shenzhen, China) and S software (coronary doc, SHUKUN Technology, Beijing, China). The raw data from the best diastolic phase of the CCTA was sent to K software in DICOM format for analysis. The CT-FFR measurement was conducted by specialists who were unaware of the other examination outcomes.

Statistical analysis
Statistical analysis was performed using SPSS software, version 24.0, developed by SPSS, Inc. based in Chicago, IL, USA. Quantitative variables were presented as Mean ± SD, whereas categorical variables were displayed as frequencies or percentages. The consistency of the two software programs was evaluated using a paired sample t-test and a Bland-Altman plot. The Bland-Altman figure showed the mean difference and ± 1.96 standard deviations as the consistency bounds. Either Pearson or Spearman correlation was utilized for the correlation analysis. The reliability was assessed using the intra-class correlation coefficient (ICC). Error classification affects were utilized for receiver operating characteristic (ROC) curve analysis. P values less than 0.05 are considered significant.

Table 2 Baseline data

Patients ($n = 72$)	Statistical description
Gender (male/female)	47/25
Age (years old)	59.85 ± 11.70
BMI (kg/m^2)	24.48 ± 3.42
HR (bpm)	60.26 ± 10.65
HRv (bpm)	17.04 ± 12.47
Hypertension (n, %)	41, 56.9%
Hyperglycemia (n, %)	18, 42.5%
Hyperlipidemia (n, %)	15, 20.8%

HR Heart rate, *HRv* Heart rate variability

Results

Baseline data

Seventy-two participants and 216 coronary vessels were included in the study. Table 2 displayed the first data.

Image quality

Subjective evaluation

72 patients were assessed for a total of 216 coronary vessels. The average score for all vessels was 3.51 with a standard deviation of 0.571. Score 1 represented 0.9% of the total (2/216); score 2 accounted for 3.7% (8/216); score 3 accounted for 41.2% (89/216); and score 4 represented 54.1% (117/216). The average scores for LAD, LCx, and RCA were 3.47 ± 0.604, 3.46 ± 0.604, and 3.60 ± 0.494, respectively.

Objective evaluation

Attenuation, noise, SNR and CNR

The attenuation of the target area was 504.85 ± 94.042 HU, the noise was 25.51 ± 9.847 HU, the SNR was 24.12 ± 12.391, and the CNR was 24.71 ± 8.323. Table 3 displays the attenuation, noise, SNR, and CNR.

Vessel shifting length

The average VSL was 0.46 mm with a standard deviation of 0.962. The LAD shifted by 0.31 ± 0.684 mm, the LCx by 0.57 ± 1.140 mm, and the RCA by 0.50 ± 1.000 mm.

Coronary LD

The average coronary LD was 3.41 mm with a standard deviation of 0.682 mm. LD_{LAD}, LD_{LCX}, and LD_{RCA} had mean diameters of 3.61 ± 0.706 mm, 3.26 ± 0.641 mm, and 3.37 ± 0.660 mm, respectively.

Coronary stenosis

The average stenosis rate of coronary artery disease was 24.68% with a standard deviation of 31.081%. Out of 216 vessels, 20.8% (15/72) were in grade I, 23.6% (17/72) were in grade II, 19.4% (14/72) were in grade III, 11.1% (8/72) were in grade IV, 20.8% (15/72) were in grade V, and 4.2% (3/72) were in grade VI.

Consistency of CT-FFR measured by different software

Paired sample t-test

A paired sample t-test was used to compare the CT-FFR readings obtained from K software and S software. The discrepancy was statistically significant with values of 0.867 ± 0.077 and 0.886 ± 0.167, $t = 2.069$, $P < 0.05$.

Bland-Altman consistency analysis

In the study population, the occurrence of ischemia was 16.2% (35/216) as determined by K software and 21.76% (47/216) as determined by S software. Figure 5 displayed the consistency results.

ICC

CT-FFR measurements using K software and S software showed a moderate level of consistency with an intraclass correlation coefficient (ICC) of 0.581 (95% confidence interval 0.452, 0.679), $P < 0.001$.

Influence factor of the difference by different CT-FFR software

Influence factor

HRv in patients showed a weak positive connection ($r = 0.226$, $P < 0.01$) with the difference in CT-FFR measurements. No other variable shows a significant correlation with the difference in the CT-FFR measurement. Subjective image quality, VSL, and LD were identified as weakly negatively correlated variables with the CT-FFR measurement difference, with correlation coefficients of

Table 3 Attenuation, noise, SNR and CNR

Parameter	Aortic root	Left coronary artery	Right coronary artery
Attenuation	(507.45 ± 85.046) HU	(516.73 ± 96.520) HU	(490.36 ± 100.56) HU
Noise	(28.91 ± 5.838) HU	(23.80 ± 10.921) HU	(23.81 ± 12.782) HU
SNR	(18.14 ± 4.056) HU	(26.43 ± 12.878) HU	(27.79 ± 20.240) HU
CNR	(21.44 ± 4.775) HU	(31.25 ± 15.419) HU	(21.44 ± 4.775) HU

SNR as signal-to-noise ratio, *CNR* as contrast-to-noise ratio

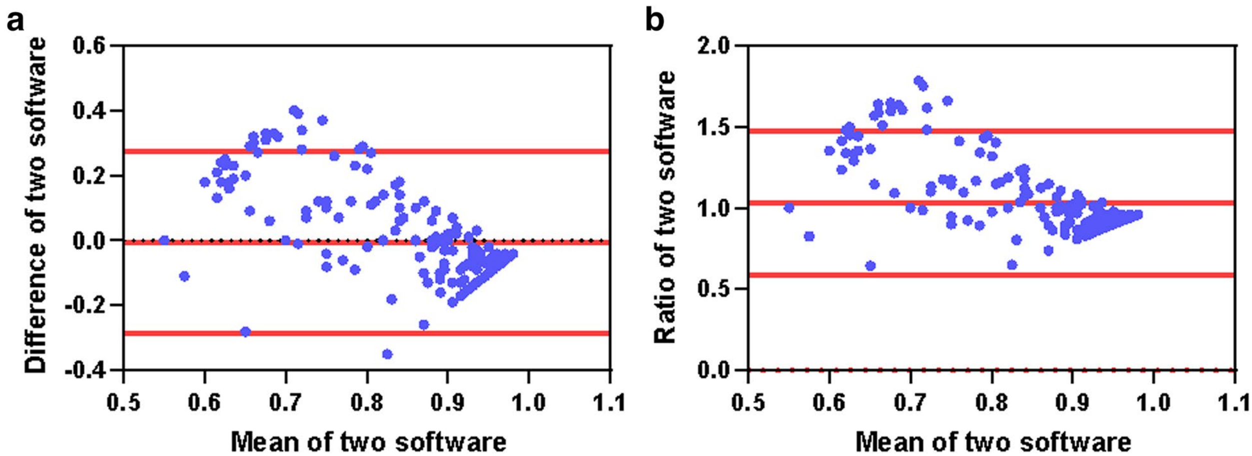

Fig. 5 Bland-Altman plots of consistency by K and S software. Note: The Bland-Altman difference plot (**a**) and ratio plot (**b**) both showed that the 6% (14 / 216) points were outside the 95% consistency limit (Fig. 5). ICC of the measurements between K and S software was 0.581, P<0.001

Table 4 Related variables analysis

Variable	Statistic	*P* value
Gender (male/female)	0.726[a]	0.469
Hypertension (yes/no)	1.815[a]	0.071
Hyperglycemia (yes/no)	0.142[a]	0.887
Hyperlipidemia (yes/no)	0.118[a]	0.696
Coronary distribution (right/others)	1.165[a]	0.248
Age (years old)	-0.028[b]	0.683
BMI (kg/m[2)]	0.060[b]	0.378
HR (bpm)	0.071[b]	0.300
HRv (bpm)	0.226[b]	0.001
VSL (mm)	0.462[b]	0.001
Attenuation (HU)	-0.037[b]	0.589
Noise (HU)	0.009[b]	0.896
SNR	-0.022[b]	0.751
CNR	-0.020[b]	0.768
LD (mm)	-0.166[b]	0.014
Coronary stenosis (%)	0.027[b]	0.695
Subjective image quality score	-0.361[c]	0.001

HR as heart rate, *HRv* as heart rate variability, *VSL* as vessel shifting length, *SNR* as signal-to-noise ratio, *CNR* as contrast-to-noise ratio, *LD* as lumen diameter

[a] As independent sample *t*-test

[b] As Pearson correlation

[c] As Spearman correlation

-0.361 ($P<0.05$), 0.462 ($P<0.01$), and -0.166 ($P<0.05$), respectively (Table 4).

ROC curve

CT-FFR values equal to or greater than 0.8 are considered negative for qualitative diagnosis, whereas values below 0.8 are considered positive. Different software correctly classified negative cases and incorrectly classified positive cases. The ROC curve is used to analyze each of the influence elements. All P values are less than 0.01 as shown in Fig. 6.

Sub-group analysis

These variables were divided into two groups according to the best cut-off points of ROC curve (0.85 mm, score of 3.5, 20 beats / min and 2.95 mm, respectively). Determine locations beyond the 95% confidence interval. The study found that the accuracy of CT-FFR measurements using various software was higher when the vessel size was less than 0.85 mm (5-12%), the image quality score was equal to or more than 3.5 (5-8%), the heart rate variability was less than 20 beats per minute (5-10%), and the lumen diameter was equal to or greater than 2.95 mm (2-6%) compared to the other group (Fig. 7).

Discussion

The investigation revealed that the discrepancy in CT-FFR measurements between K software and S software exceeded the 95% consistency limit in the Bland-Altman plot. It demonstrates that the measurements obtained from several software programs are inconsistent. Subsequent studies have revealed numerous parameters that influence variability in CT-FFR measurements with different software, such as heart rate variability, subjective image quality, vessel signal-to-noise ratio, and lumen diameter. The VSL has the highest AUC, with the optimal cut-off point being 0.85 mm. When the vessel shifting distance exceeded 0.85 mm, there was a notable rise in

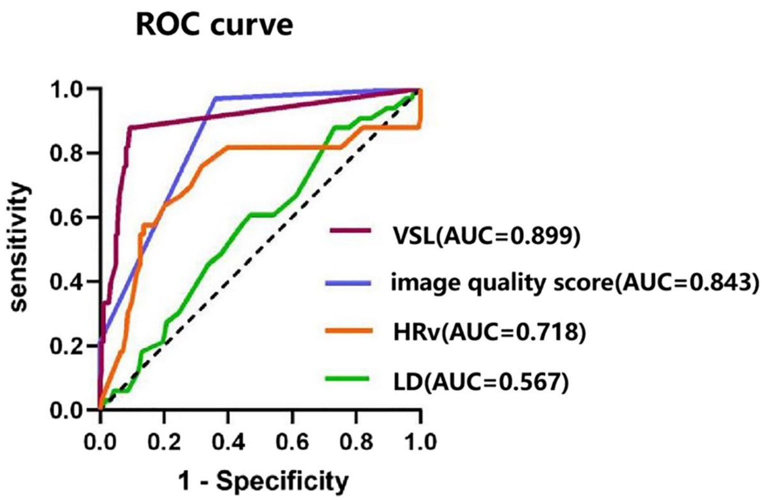

Fig. 6 ROC curves of diagnosis classification. Note: The optimal cut-off point of HRv was 20 times /min, the sensitivity was 75.8%, the specificity was 68.3%. The the cut-off point of VSL was 0.85 mm, the sensitivity was 87.9%, the specificity was 90.7%. The optimal cut-off point of subjective image quality score was 3.5 points, the sensitivity was 63.5%, the specificity was 91%. The optimal cut-off point of LD was 2.95 mm, the sensitivity was 87.9%, the specificity was 27.1%

the discrepancy of CT-FFR measurements obtained from different software.

Artificial intelligence (AI) and machine learning (ML) are widely used in various fields and improve robustness and generalization capability through varioustechniques [19–23]. CT-FFR utilizes a multi-layer neural network framework to construct a coronary artery database based on the anatomical structure and hydrodynamics of the coronary artery tree. It has shown benefits in terms of processing speed and greatly enhanced work productivity. CT-FFR showed comparable diagnostic efficacy to invasive FFR. It greatly enhanced the detection of ischemic lesions resulting from obstructive stenosis and reassessed the level of ischemia [24, 25]. The variation in CT-FFR measurements from different software was influenced by technological differences [6, 26–28]. The study results were consistent with the present software's application state. The basic data for CT-FFR comes from CCTA and one of the key steps is to build a coronary tree model through CCTA. Image segmentation has been a fundamental component of medical image analysis for an extensive period. The primitive image features (e.g., pixel intensities and edge maps) significantly impacts their robustness and generalization capability [29, 30]. Analyzed in a multicenter retrospective investigation, factors influencing CT-FFR included subjective picture quality, objective image quality, and heart rate, affecting its diagnostic accuracy. Subjective image quality score ≥ 3 points, attenuation between 300 and 400 HU, and heart rate less than 70 bpm were found to enhance the credibility of CT-FFR [31]. The current survey indicates that image quality, lumen diameter, and HRv are significant factors that influence the CT-FFR calculations evaluated with various software, yielding comparable results. Criteria for guaranteeing measurement stability included a lumen diameter of 2.95 mm or above, HRv less than 20 bpm, subjective image quality score of 3.5 points or higher, and VSL less than 0.85 mm. Xu et al. [32] propose a multi-feature fusion method to identify high-risk plaque. The proposed method helped to build a more complete feature set so that the machine learning models could identify vulnerable plaque more accurately even on datasets with poor quality. In future studies, we will continue to explore the effect of image quality on coronary hemodynamics. Heart rate variability (HRv) can cause variations in the heart's diastole and systole, leading to irregular acquisition positions. An increase in HRv may lead to a rise in phase difference, which might affect image registration differences [33, 34]. In this study, 7.7% (6 out of 78) patients were unable to have their CT-FFR

(See figure on next page.)

Fig. 7 Bland-Altman plots of sub-group analysis. Note: Figure **a** showed the Bland Altman plot with VSL ≥ 0.85 mm, which showed that the 12% (6/51) points were outside the 95% confidence interval; 5% (8/165) if VSL < 0.85 mm (**b**) Figure **c** showed the Bland Altman plot with Subjective image quality score < 3.5, which showed that the 8%(9/118) points were outside the 95% confidence interval; 5% (5/98) if the score ≥ 3.5 (**d**) Figure **e** showed the Bland Altman plot with HRv ≥ 20 bpm, which showed that the 10% (12/116) points were outside the 95% confidence interval; 5% (5/100) if HRv < 20 bpm (**f**) Figure **g** showed the Bland Altman plot with LD ≥ 2.95 mm, which showed that the 2%(3/164) points were outside the 95% confidence interval; 6% (3/52) if the LD< 2.95 mm (**h**)

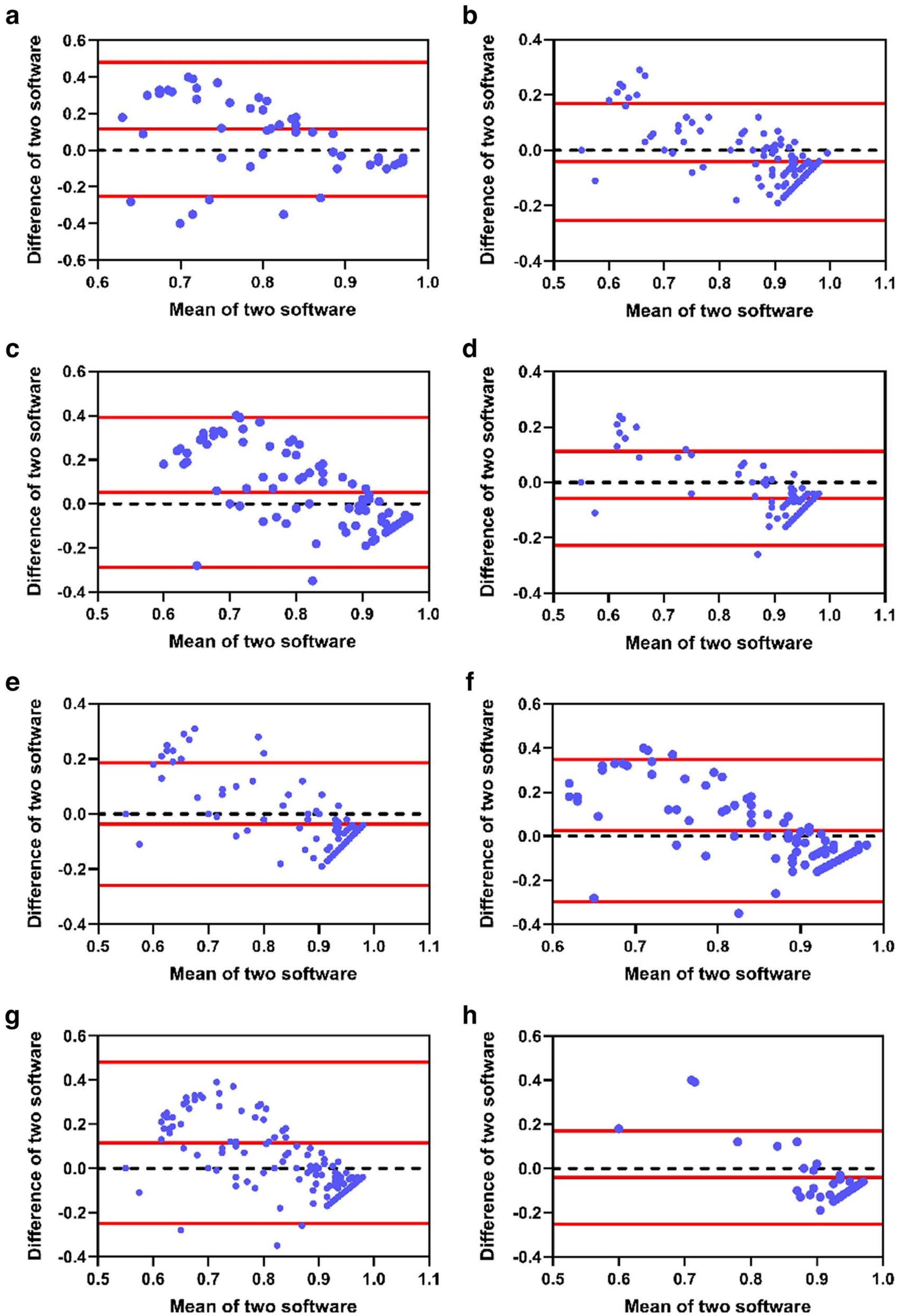

Fig. 7 (See legend on previous page.)

estimated using the K program due to image registration discrepancies. Some scholars tested two dynamic registration methods to correct for the patient respiratory movements [35]. In this study, respiratory movement has a more direct impact on subjective image quality, and patient respiratory coordination is extremely important. Hence, achieving optimal image quality is crucial in the clinical application of CT-FFR.

The hydrodynamic model of CT-FFR relies on precise image data and the boundary of the vessel wall. Elevated heart rate can cause motion abnormalities and inadequate dilation of the coronary arteries [36]. Xu et al. [31] showed that the specificity and positive predictive value of CT-FFR were greater at low heart rates compared to high heart rates. The ADVANCE study [37] demonstrated that heart rate independently predicted the quality of CCTA images. This suggests that the heart rate can affect the visualization of coronary arteries. The DeFACTO study discovered that β-Receptor blockers or nitroglycerin could notably enhance the specificity of CT-FFR [38]. The study utilized a second-generation dual-source CT scanner with high temporal resolution and scanning speed, ensuring minimal impact on image quality from heart rate variations. Our investigation did not demonstrate the impact of heart rate on the consistency of CT-FFR measurement. To ensure accurate CT-FFR values, it was essential to regulate the heart rate during the CCTA examination.

The investigation revealed that the lumen diameter has an impact on measurement consistency. The lumen diameter may affect the fine resolution. The size of the lumen has an impact on the precision of morphological diagnosis [39]. Sankaran and colleagues examined how the uncertainty of minimum lumen diameter, lesion length, boundary resistance, and blood viscosity affect FFR. The study findings indicated that the impact of minimal lumen width on CT-FFR was greater than that of other variables such as lesion length, viscosity, and border resistance [37]. In this study, the examination of several components did not find the lumen diameter to be a statistically significant determinant. Our investigation concluded that coronary stenosis did not have a major impact on the variations caused by different software. This suggests that there may not be a clear connection between coronary stenosis and the hemodynamic alterations.

Future studies involving more clinical data will be necessary to verify the stability of CT-FFR measurements with different softwares and relevant influence factors in order to provide reliable guarantees for CT-FFR evaluation of myocardial ischemia.

Our study has some limitations. First, the study was limited by a small sample size, which could result in type I errors and limits the statistical power and strength of the conclusions. In the future, it is necessary to further enhance the sample size to confirm the dependability and correctness of the research results. Second, invasive fractional flow reserve is a crucial clinical benchmark for assessing the function of CAD. In this study, the small number of patients undergoing iFFR intervention made it difficult to support subsequent analysis. In later studies, iFFR should be further used as a standard to compare the clinical efficacy of different software in evaluating hemodynamics while expanding the sample size. Third, the S software lacks approval from the National Medical Products Administration and may have inadequate clinical validation.

Conclusions

Our study demonstrates that there are significant variations in the CT-FFR measurements produced by different software providers and even qualitative diagnostic misclassifications occur. Various software stability was influenced by lumen diameter, HRv, subjective image quality score, and VSL. We recommend carefully considering the variations among different software in clinical practice and selecting optimal measurement software based on clinical practice. In the actual clinical work, it is necessary to pay attention to the influencing factors related to image quality, and it is also necessary to carefully interpret the guidance of CT-FFR in evaluating the degree of cardiac ischemia. Future multicenter prospective studies will be necessary for the validation of our findings.

Abbreviations

CT-FFR	Computed tomography fractional flow reserve
CCTA	Coronary computed tomography angiography
CAD	Coronary artery disease
CFD	Computational fluid dynamics
ROI	Region of interest
CPR	Curved planar reconstruction
MIP	Maximum intensity projection
VRT	Volumetric rendering technique
MPR	Multi-planar reformation
AO	Aortic root
SD	Standard deviation
SNR	Signal-to-noise ratio
CNR	Contrast-to-noise ratio
VSL	Vessel shifting length
LD	Lumen diameter
SCCT	Society of Cardiovascular Computed Tomography

Acknowledgements

Not applicable.

Authors' contributions

JL: conceptualization, data curation, manuscript draft, and editing. ZY: data acquisition, data analysis, manuscript draft. ZS: Visualization, Investigation. XW: data acquisition, data analysis. QJ: data acquisition, data analysis. GZ: data acquisition, data analysis. LZ and AL: conceptualization, manuscript draft and editing, supervision of of the research group. All authors read and approved the final manuscript.

Funding
This study has received funding by Inner Mongolia Medical University Research Program Project:
The Inner Mongolia Medical University youth project (YKD2024QN026).

Data availability
The datasets used and analysed during the current study available from the corresponding author on reasonable request.

Declarations

Ethics approval and consent to participate
The study was approved by the Research Ethics Board of Affiliated Hospital of Inner Mongolia Medical University. The requirement of informed consent from the patients was waived by the Research Ethics Board of Affiliated Hospital of Inner Mongolia Medical University. All methods were carried out in accordance with the Declaration of Helsinki.

Consent for publication
Not applicable.

Competing interests
The authors declare no competing interests.

Author details
[1]Department of Radiology, the Affiliated Hospital of Inner Mongolia Medical University, No.1 Tongdao North Street, Hohhot, Inner Mongolia 010050, China. [2]Department of Basic Medicine College, Inner Mongolia Medical University, No.5 Tongdao North Street, Hohhot, Inner Mongolia 010059, China. [3]Department of Mathematics College, Inner Mongolia University, Daxue West Street, Hohhot, Inner Mongolia 010020, China.

Received: 22 July 2024 Accepted: 15 October 2024
Published: 24 October 2024

References
1. Go AS, Mozaffarian D, Roger VL, Benjamin EJ, Berry JD, Blaha MJ, Dai S, Ford ES, Fox CS, Franco S, et al. Heart disease and stroke statistics–2014 update: a report from the American Heart Association. Circulation. 2014;129:e28-92.
2. Sechtem U, Seitz A, Ong P, Bekeredjian R. Management of chronic coronary syndrome. Herz. 2019;47:472–82.
3. Gao Z, Wang X, Sun S, et al. Learning physical properties in complex visual scenes: an intelligent machine for perceiving blood flow dynamics from static CT angiography imaging. Neural Netw. 2019;123:82–93.
4. Baumann S, Hirt M, Schoepf UJ, et al. Correlation of machine learning computed tomography-based fractional flow reserve with instantaneous wave free ratio to detect hemodynamically significant coronary stenosis. Clin Res Cardiol. 2019;109:735–45.
5. Dobrić M, Furtula M, Tešić M, et al. Current status and future perspectives of fractional flow reserve derived from invasive coronary angiography. Front Cardiovasc Med. 2023;10: 1181803.
6. Fujii Y, Kitagawa T, Ikenaga H, Tatsugami F, Awai K, Nakano Y. The reliability and utility of on-site CT-derived fractional flow reserve (FFR) based on fluid structure interactions: comparison with FFR based on computational fluid dynamics, invasive FFR, and resting full-cycle ratio. Heart Vessels. 2023;38:1095–107.
7. Guan X, Song D, Li C, et al. Functional assessment of coronary artery stenosis from coronary angiography and computed tomography: angio-FFR vs. CT-FFR. J Cardiovasc Transl Res. 2023;16:905–15.
8. Lattice-Boltzmann interactive. Blood flow simulation pipeline[J]. Int J Comput Assist Radiol Surg. 2020;15(4):629–39.
9. Zhai X, Amira A, Bensaali F, et al. Zynq SoC based acceleration of the lattice Boltzmann method. Concurrency Comput Pract Exp. 2019;31(17):e5184.1-e5184.10.
10. Xiaojun Z, Minsi, et al. Heterogeneous system-on-chip-based Lattice-Boltzmann visual simulation system. IEEE Syst J. 2019;14(2):1592–601.
11. Bray JJH, Hanif MA, Alradhawi M, et al. Machine learning applications in cardiac computed tomography: a composite systematic review. Eur Heart J Open. 2022;2:oeac018.
12. Tesche C, De Cecco CN, Baumann S, et al. Coronary CT angiography-derived fractional flow reserve machine learning algorithm versus computational fluid dynamics modeling. Radiology. 2018;288:64–72.
13. Li Y, Qiu H, Hou Z, et al. Additional value of deep learning computed tomographic angiography-based fractional flow reserve in detecting coronary stenosis and predicting outcomes. Acta Radiol. 2022;63:133–40.
14. Itu L, Rapaka S, Passerini T, et al. A machine-learning approach for computation of fractional flow reserve from coronary computed tomography. J Appl Physiol. 2016;121:42–52.
15. Li S, Nunes JC, Toumoulin C, et al. 3D Coronary Artery Reconstruction by 2D motion compensation based on mutual Information. Irbm. 2018;39(1):69–82.
16. Mark DB, Berman DS, Budoff MJ, ACCF / ACR / AHA / NASCI / SAIP / SCAI / SCCT, et al. 2010 expert consensus document on coronary computed tomographic angiography: a report of the American College of Cardiology Foundation Task Force on Expert Consensus documents. Catheter Cardiovasc Interv. 2010;76:E1-42.
17. Chen Z, Contijoch F, Schluchter A, et al. Precise measurement of coronary stenosis diameter with CCTA using CT number calibration. Med Phys. 2019;46:5514–27.
18. Cury RC, Leipsic J, Abbara S, et al. CAD-RADS™ 2.0–2022 Coronary Artery Disease - Reporting and Data System: An expert consensus document of the Society of Cardiovascular Computed Tomography (SCCT), the American College of Cardiology (ACC), the American College of Radiology (ACR) and the North America Society of Cardiovascular Imaging (NASCI). J Am Coll Radiol. 2022;19:1185–212.
19. Mohtasebi M, Bayat M, Ghadimi S, et al. Modeling of neonatal skull development using computed tomography images. IRBM. 2020. https://doi.org/10.1016/j.irbm.2020.02.002.
20. Balasubramanian K, Ananthamoorthy NP. Robust retinal blood vessel segmentation using convolutional neural network and support vector machine. J Ambient Intell Humaniz Comput. 2019. https://doi.org/10.1007/s12652-019-01559-w.
21. Belderrar A, Hazzab A. Real-time estimation of hospital discharge using fuzzy radial basis function network and electronic health record data. Int J Med Eng Inf. 2021;13(1):75.
22. Re-routing drugs to. Blood brain barrier: a comprehensive analysis of machine learning approaches with fingerprint amalgamation and data balancing. IEEE Access. 2023;11:9890–906.
23. Ansari MY, Yang Y, Meher P, et al. Dense-PSP-UNet: a neural network for fast inference liver ultrasound segmentation. Comput Biol Med. 2022;153:106478.
24. An Z, Tian J, Zhao X, et al. Machine learning-based CT angiography-derived fractional flow reserve for diagnosis of functionally significant coronary artery disease. JACC Cardiovasc Imaging. 2023;16:401–4.
25. Xue J, Li J, Sun D, et al. Functional evaluation of intermediate coronary lesions with integrated computed tomography angiography and invasive angiography in patients with stable coronary artery disease. J Transl Int Med. 2022;10:255–63.
26. Wang ZQ, Zhou YJ, Zhao YX, et al. Diagnostic accuracy of a deep learning approach to calculate FFR from coronary CT angiography. J Geriatr Cardiol. 2019;16:42–8.
27. Wang W, Wang H, Chen Q, et al. Coronary artery calcium score quantification using a deep-learning algorithm - ScienceDirect. Clin Radiol. 2020;75:e23711-23716.
28. Tesche C, Gray HN. Machine learning and deep neural networks applications in coronary flow assessment: the case of computed tomography fractional flow reserve. J Thorac Imaging. 2020;35(Suppl 1):S66-71.
29. Zhai X, Eslami M, Hussein ES, et al. Real-time automated image segmentation technique for cerebral aneurysm on reconfigurable system-on-chip. J Comput Sci. 2018;27(JUL):35–45.
30. Ansari MY, Yang Y, Balakrishnan S, et al. A lightweight neural network with multiscale feature enhancement for liver CT segmentation. Scientific Reports, Nature. 2022;12:14153.
31. Xu PP, Li JH, Zhou F, et al. The influence of image quality on diagnostic performance of a machine learning-based fractional flow reserve derived from coronary CT angiography. Eur Radiol. 2020;30:2525–34.

32. Xu X, Wu R, Zhang W, Ding G, Xie J, Huang L, Liu L, Chi M. Multi-Feature Fusion Method for Identifying Carotid Artery Vulnerable Plaque. Innovation and research in biomedical engineering: IRBM. 2022;43(4):272–8.
33. Gordic S, Husarik DB, Desbiolles L, Leschka S, Frauenfelder T, Alkadhi H. High-pitch coronary CT angiography with third generation dual-source CT: limits of heart rate. Int J Cardiovasc Imaging. 2014;30:1173–9.
34. Chen Y, Wei D, Li D, et al. The value of 16-cm wide-detector computed tomography in coronary computed tomography angiography for patients with high heart rate variability. J Comput Assist Tomogr. 2018;42:906–11.
35. Cohen ME, Pellot-Barakat C, Tacchella JM, et al. Quantitative evaluation of rigid and elastic registrations for abdominal perfusion imaging with X-ray computed tomography. Irbm. 2013;34(4–5):283–6.
36. Ondrejkovic M, Salat D, Cambal D, Klepanec A. Radiation dose and image quality of CT coronary angiography in patients with high heart rate or irregular heart rhythm using a 16-cm wide detector CT scanner. Med (Baltim). 2022;101:e30583.
37. Sankaran S, Kim HJ, Choi G, Taylor CA. Uncertainty quantification in coronary blood flow simulations: impact of geometry, boundary conditions and blood viscosity. J Biomech. 2016;49:2540–7.
38. Gonzalez JA, Lipinski MJ, Flors L, Shaw PW, Kramer CM, Salerno M. Meta-analysis of diagnostic performance of coronary computed tomography angiography, computed tomography perfusion, and computed tomography-fractional flow reserve in functional myocardial ischemia assessment versus invasive fractional flow reserve. Am J Cardiol. 2015;116:1469–78.
39. Yan RT, Miller JM, Rochitte CE, et al. Predictors of inaccurate coronary arterial stenosis assessment by CT angiography. JACC Cardiovasc Imaging. 2013;6:963–72.

Publisher's note